Importance of van der Waals Interactions in QM/MM Simulations

Demian Riccardi, Guohui Li, and Qiang Cui*

Department of Chemistry and Theoretical Chemistry Institute, University of Wisconsin, Madison, 1101 University Ave, Madison, Wisconsin 53706

Received: December 23, 2003; In Final Form: March 1, 2004

The importance of accurately treating van der Waals interactions between the quantum mechanical (QM) and molecular mechanical (MM) atoms in hybrid QM/MM simulations has been investigated systematically. First, a set of van der Waals (vdW) parameters was optimized for an approximate density functional method, the self-consistent charge-tight binding density functional (SCC-DFTB) approach, based on small hydrogen-bonding clusters. The sensitivity of condensed phase observables to the SCC-DFTB vdW parameters was then quantitatively investigated by SCC-DFTB/MM simulations of several model systems using the optimized set and two sets of extreme vdW parameters selected from the CHARMM22 forcefield. The model systems include a model FAD molecule in solution and a solvated enediolate, and the properties studied include the radial distribution functions of water molecules around the solute (model FAD and enediolate), the reduction potential of the model FAD and the potential of mean force for an intramolecular proton transfer in the enediolate. Although there are noticeable differences between parameter sets for gas-phase clusters and solvent structures around the solute, thermodynamic quantities in the condensed phase (e.g., reduction potential and potential of mean force) were found to be less sensitive to the numerical values of vdW parameters. The differences between SCC-DFTB/MM results with the three vdW parameter sets for SCC-DFTB atoms were explained in terms of the effects of the parameter set on solvation. The current study has made it clear that efforts in improving the reliability of QM/MM methods for energetical properties in the condensed phase should focus on components other than van der Waals interactions between QM and MM atoms.

1. Introduction

The analysis of chemical events in complex systems requires a potential function that can describe electronic changes in the region of interest. Current quantum mechanical approaches provide such descriptions, but there are severe limitations in the size of the systems that can be treated.[1,2] To investigate the effects of the environment on chemical events, approximations must be made with either an implicit or explicit approach. For biological systems, the inclusion of the protein and solvent environment is paramount,[3] and combined quantum mechanical and molecular mechanical (QM/MM) methods[4−6] are a popular choice for such investigations. QM/MM methods enable theoretical computations of complex chemical events in large systems by partitioning the system into a quantum region and a molecular mechanics region. The application of the QM/MM method can provide atomistic details of catalytic mechanisms corresponding to experimental observables, which is valuable for both fundamental understanding of enzyme catalysis and realistic applications such as protein engineering.

The total Hamiltonian for the molecular system under consideration in the QM/MM framework is

$$\hat{H} = \hat{H}^{\mathrm{QM}} + \hat{H}^{\mathrm{QM/MM}} + \hat{H}^{\mathrm{MM}} \tag{1}$$

where $\hat{H}^{\mathrm{QM/MM}}$ describes the interaction between the QM and MM atoms governed by $\hat{H}^{\mathrm{QM}}$ and $\hat{H}^{\mathrm{MM}}$, respectively. The $\hat{H}^{\mathrm{QM/MM}}$ typically contains terms for the electrostatic, van der Waals(vdW), and bonded interactions

$$\hat{H}^{\mathrm{QM/MM}} = \hat{H}^{\mathrm{QM/MM}}_{\mathrm{vdW}} + \hat{H}^{\mathrm{QM/MM}}_{\mathrm{elec}} + \hat{H}^{\mathrm{QM/MM}}_{\mathrm{bonded}} \tag{2}$$

The $\hat{H}^{\mathrm{QM/MM}}_{\mathrm{bonded}}$ is required when partitioning a single molecule into quantum and molecular mechanics regions, as is most common for applications to protein systems. For such partitioning, the molecular mechanical bonding term is retained between the boundary QM and MM atoms, whereas the valency of the QM region is satisfied with the addition of link atoms[4] or frontier bonds.[7,8] The purpose of the vdW term is to estimate dispersion attractions that fall off as r^{-6} and to prevent molecular collapse being strongly repulsive at short interaction distances. In terms of the magnitudes at typical interactomic distances, electrostatic interactions usually overwhelm the vdW contributions, especially in polar systems such as enzymes. Due to the rapid variation at short interatomic distances, however, the vdW interactions (therefore vdW parameters) are important to the equilibrium geometries of molecules treated by QM/MM in the gas phase.[4,9−12] In the condensed phase, on the other hand, due to averaging over a large number of configurations, the question of how important the precision of QM/MM van der Waals interactions is to the molecular properties of common interest is an interesting one, which has not been systematically explored in the past. Moreover, the vdW interaction between QM and MM atoms in the condensed phase may not only affect the enthalpy of direct interactions but also have a substantial entropic component, and the possibility of enthalpy/entropy compensation has not been analyzed in details in previous work.

In the current paper, we report a systematic analysis on the

* To whom the correspondence should be addressed.

10.1021/jp037992q CCC: $27.50
Published on Web 04/23/2004

importance of van der Waals interactions in QM/MM simulations, with emphasis on condensed phase properties, which we believe is an indispensable step toward developing quantitative QM/MM methods for studying complex systems. The work consists of two major components. First, we realize that the $\hat{H}_{vdW}$ contains the most readily adjustable parameters, and the implementation of new quantum mechanical methods to existing MM force fields requires the optimization of these parameters.[4] Recently, an approximate density functional approach termed the self-consistent-charge density-functional-tight-binding method (SCC-DFTB)[13] has been introduced and implemented into the CHARMM package for QM/MM calculations.[14] Although SCC-DFTB/MM investigations have produced useful mechanistic insights for several enzyme systems,[15−17] the vdW parameters have yet to be optimized for more quantitative studies. In this investigation, to improve the performance of SCC-DFTB/CHARMM calculations, we have optimized the vdW parameters for SCC-DFTB atoms (C, O, N, and H) using a set of hydrogen bonding complexes chosen to represent the interaction of selected amino acid side chains with water molecules. We verify that the parameters are transferable between similar atomic environments in different molecules.

Next, a systematic comparison between the optimized vdW parameters (set Opt) and two extreme sets (set A and set B, see section 2) of parameters taken from the CHARMM force field is made for gas-phase interactions and condensed phase observables to determine the sensitivity of these observables with respect to the parameters in SCC-DFTB/MM simulations. Although the comparison of computational with experimental results is paramount for realistic applications, the goal of this analysis is not to compare with experiment but rather to determine the variation of observables with QM vdW parameters. In the following, we will describe the computational methods and simulation details in section 2 and the results and discussion in section 3. This work will be summarized with conclusions in section 4.

2. Computational Methods

2.1. QM/MM Energy Evaluation. According to eq 1, the energy of QM/MM simulations is determined by combining the Hamiltonians of the quantum mechanical and molecular mechanical regions with a QM/MM coupling term composed of electrostatic, bonded, and van der Waals contributions

$$U_{tot} = \langle\Psi|\hat{H}^{QM} + \hat{H}^{QM}_{elec}|\Psi\rangle + U^{QM/MM}_{vdW} + U^{QM/MM}_{bonded} + U^{MM} \quad (3)$$

The QM approach used here is SCC-DFTB,[13] which is very efficient due mainly to approximations to the two-electron integrals. This method introduces the charge self- consistency at the level of Mulliken population and, accordingly, the QM atoms interact with the MM sites electrostatically through Mulliken partial charges[14]

$$U^{QM/MM}_{elec} = \sum_{A\in MM}\sum_{B\in QM}\frac{Q_A\Delta q_B}{|\mathbf{R}_A - \mathbf{R}_B|} \quad (4)$$

where Q_A and Δq_B are the MM partial charges and Mulliken partial charges, respectively. We note that although other definitions of charges in SCC-DFTB and SCC-DFBT/MM calculations can in principle be used instead of the simple Mulliken charges, important parameters in SCC-DFTB (e.g., repulsive potentials) were optimized within the Mulliken framework.[13,18] Therefore, improvement in the accuracy of SCC-DFTB by adopting more sophisticated charges (e.g., NBO charges[19]) is likely to be limited. One crucial limitation of using Mulliken charges in $U^{QM/MM}_{elec}$ is that the anisotropy of interactions tends to be underestimated (see section 3).

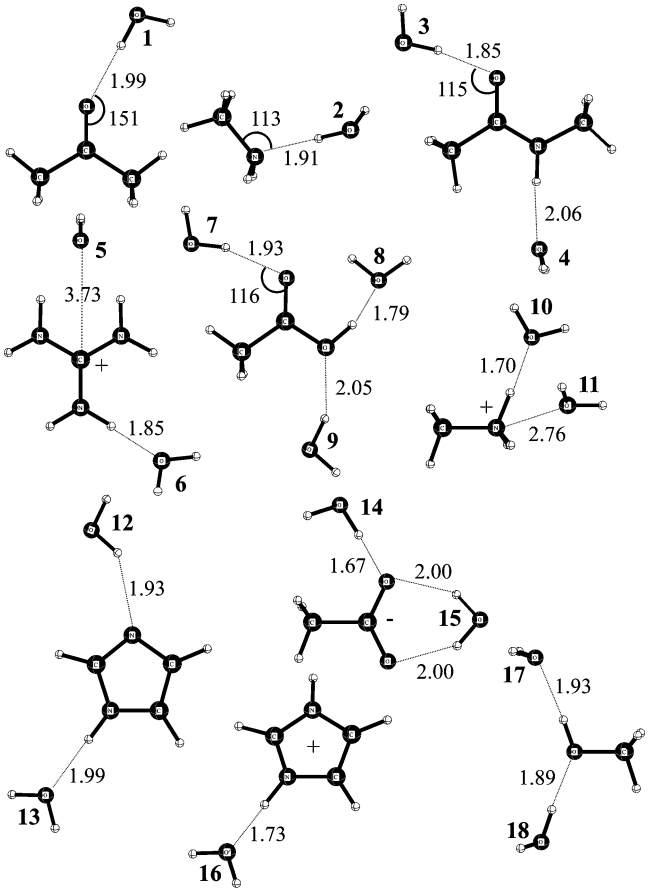

Figure 1. Training set molecules. These complexes were chosen to represent typical amino acid side chain interactions with water. This set was used fot the optimization of the van der Waals parameters for SCC-DFTB atom as required for SCC-DFTB/MM calculations, treating the organic molecule with SCC-DFTB and the water with TIP3P. The reference stationary point geometries presented here were optimized at the B3LYP/6-31+G** level. Distances are in angstroms, and angles are in degrees.

The vdW term consists of predetermined parameters described by

$$U^{QM/MM}_{vdW} = \sum_{A\in MM}\sum_{B\in QM}\epsilon_{AB}\left[\left(\frac{\sigma_{AB}}{R_{AB}}\right)^{12} - 2\left(\frac{\sigma_{AB}}{R_{AB}}\right)^{6}\right] \quad (5)$$

where A and B are the indices for the MM and QM nuclei, respectively, and R_{AB} is the distance between QM and MM nuclei. The vdW parameters are defined by the standard combination rules: $\epsilon_{AB} = (\epsilon_A\epsilon_B)^{1/2}$ and $\sigma_{AB} = 1/2(\sigma_A + \sigma_B)$, where ϵ and σ describe the well depth and atomic radius, respectively. Different QM methods require, in principle, different vdW parameters for optimal results,[10,9] and the optimization of these parameters for SCC-DFTB is the first goal in this investigation. This will be followed by a systematic study on the quantitative importance of the precision of QM/MM van der Waals interactions to results.

2.2. Optimization of van der Waals Parameters. A training set of hydrogen bonded complexes (see Figure 1) were used to optimize the vdW parameters for SCC-DFTB atoms in eq 5. In

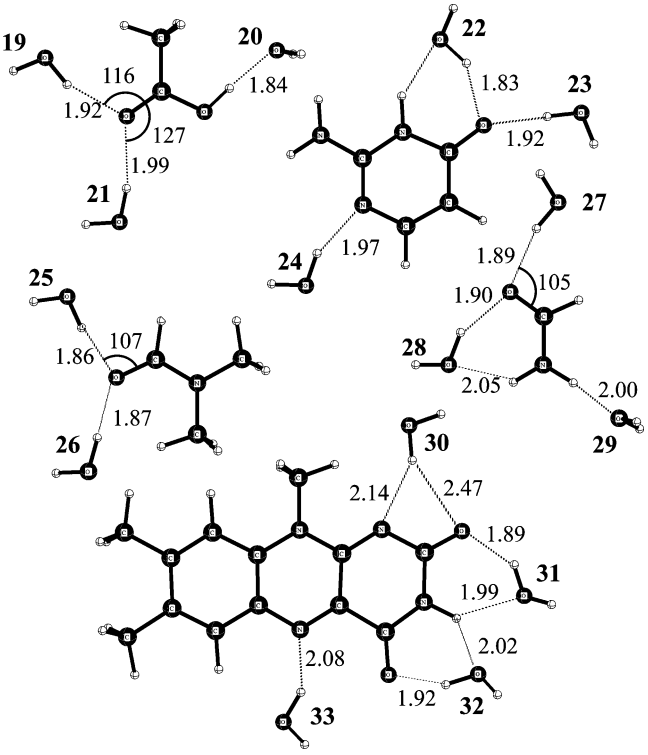

Figure 2. Complexes not included in the optimization of the van der Waals parameters for SCC-DFTB atoms. The stationary point geometries presented here were optimized at the B3LYP/6-31+G** level. These molecules were chosen as to represent similar hydrogen bonding interactions in complexes that were different from the training set to test the transferability of the van der Waals parameters treating the organic molecule with SCC-DFTB and the water with TIP3P. Distances are in angstroms, and angles are in degrees.

addition to the training set, a set of hydrogen bonded complexes not used in the parameter opimization (see Figure 2) were used to verify the transferability of the parameters. The complexes were chosen to capture amino acid interactions with water; a subset of the complexes were used previously by M. Freindorf and J. Gao in the optimization of vdW parameters for the HF/3-21G/MM potential.[10] We note that eq 5 is in a simplified form, as in practice the vdW contribution would be limited to atoms found within a defined cutoff.[20]

For all of the gas-phase complexes (Figures 1 and 2), the water molecule was treated with MM using a modified TIP3P model, as implemented in CHARMM,[21] whereas the organic molecule was treated with SCC-DFTB. To ensure the largest transferrability, the vdW parameters were chosen to depend only on the element type rather than atom type. The exception was made for hydrogen, for which only the vdW parameters for polar hydrogen atoms were optimized; for nonpolar hydrogen, the standard CHARMM parameters were used. The vdW parameters for C, O, N, and (polar) H were varied using a genetic algorithm (GA)[22] to determine a set that maximized the "fitness". The fitness (χ) is defined as the inverse of a weighted sum of differences between values determined from the SCC-DFTB/MM and the reference calculations:

$$\chi = \frac{\sum_{i=1} w_i \left[Y_i(\text{reference}) - Y_i(\text{SCC} - \text{DFTB/MM})\right]^2}{\sum_{i=1} w_i} \quad (6)$$

where i is the index of the complex and the sum is over all properties for all complexes. The properties included in χ consist of vertical hydrogen bond energies and the gradient for the hydrogen bond distance and angle (should be zero at a stationary point). For the SCC-DFTB/MM values, a finite difference apporach was used to determine the gradient about the hydrogen bond distances (0.02Å deviation) and angles (2.0° deviation) associated with the reference structure (B3LYP/6-31+G**). Although the analytical gradient was available for SCC-DFTB/MM,[14] the finite difference approach proved more convenient here for the GA optimization.

The reference values were determined from B3LYP[23−25] calculations using B3LYP/6-31+G** for geometry optimizations and B3LYP/6-311++G**[26,27] for single-point energy evaluations for each complex. The reliability of density functional theories for describing hydrogen bonded complexes has been discussed rather extensively in the literature.[28,29] Although it is well-known that local DFT methods tend to overestimate intermolecular interactions, calculations using nonlocal functionals (especially hybrid functionals) were found to be actually rather reliable compared to high level ab initio methods. For example, an early study by Salahub and co-workers[28] on prototypical hydrogen-bonding complexes such as water dimer and formamide−water clusters found that DFT calculations using several popular nonlocal functionals agreed well with MP2 and experimental results. More recently, Jorgensen and co-workers[29] have compared the performance of the popular B3LYP method, MP2, and various high-level extrapolation-based methods (CBS)[30] for more than 50 hydrogen bonding complexes involving organic molecules and water. It was also found that the performance of B3LYP was quite impressive compared to more sophisticated calculations, provided that basis sets larger than 6-31+G** are used. Therefore, although it is crucial to remember that dispersion interaction is missing from popular implementations of DFT and could be important in many occasions of biological significance (e.g., nucleic acid base stacking[31]), one should note that B3LYP with a decent basis set is a fairly robust approach for treating typical hydrogen-bonding interactions (∼10 kcal/mol).

In the genetic algorithm, weighting (w_i in eq 6) was used to adjust the sensitivity of selected properties to the optimization; for this study, weights of 3.0, 5.0, and 1.0 were used for the interaction energies, hydrogen bond angles, and distances, respectively. The different weights were chosen so that the interaction energy evaluation was the most important followed by the gradient calculations (where the gradient about the angle needed a higher weight to compensate its smaller value in units of kcal/mol·degree). Similar results were obtained for minimizations with different weights. During the GA optimization, consistent vdW values were found with various GA settings; the values reported here were obtained with a micro-GA technique with a population of 5 chromosomes that was allowed to operate for 400 generations with uniform crossovers, see ref 32 for detailed descriptions and recommendations for the GA options.

2.3. Gas-Phase Comparisons. Hydrogen bond distances and energies were compared between the full B3LYP, full SCC-DFTB, and SCC-DFTB/MM with opimized vdW parameters. In addition, SCC-DFTB/MM calculations were also carried out with two "extreme" sets, one with "maximal" vdW interaction parameters (set A) and one with "minimal" vdW interaction parameters (set B). The values for sets A and B were taken directly from the CHARMM22[21] force field selected in such a way that set A contains the smallest σ_{AB} and largest ϵ_{AB} to promote closer packing, whereas set B contains the largest σ_{AB}

SCHEME 1

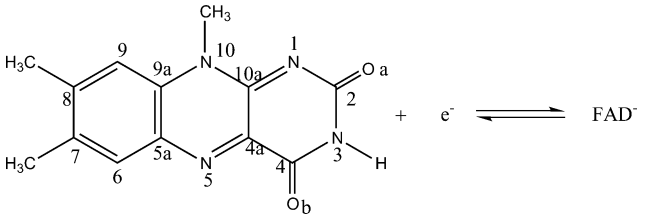

SCHEME 2

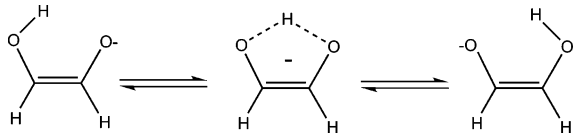

and smallest ϵ_{AB} thereby pushing out the MM solvent providing a molecular surface that would tend to be more "slippery". The gas-phase comparisons were made for both the training set (see Figure 1) and the set of hydrogen bonded complexes not used in the parameter optimization (see Figure 2).

2.4. Condensed Phase Observables. To determine the effect of vdW parameters on condensed phase observables, a series of free energy and potential of mean force (PMF) calculations were carried out using the SCC-DFTB/MM approach described above with each of the three sets of vdW parameters. The free energy and PMF calculations were chosen because they are the typical type of simulations that characterize energetics of chemical events in the condensed phase. The free energy was determined for the process of reducing the isoalloxazine ring of flavin adenine dinucleotide (FAD, see Scheme 1) in solution using a thermodynamic integration scheme; this was compared to the gas-phase potential energy difference to determine the energetic effect of solvation. The PMF was determined for the proton-transfer process in a model enediolate in solution (see Scheme 2).

2.4.1. Reduction Potential of a Model FAD. All free energy calculations for the model FAD reduction were carried out with CPT[33] molecular dynamics under periodic boundary conditions. An FAD molecule was solvated in a 38 Å water box with 1769 water molecules. The nonbond interactions were determined on an atom−atom pair basis with pair interactions terminated at 12 Å and reduced to zero at 12 Å using a shift function with a dielectric constant of one. Bonds involving hydrogen were constrained using the SHAKE algorithm;[34] the system was heated to 285, 300, or 325 K (see below) and equilibrated for 50 ps. The free energy derivatives were calculated with a thermodynamic integration method[35] until convergence (usually about 200 ps) was achieved for three windows ($\lambda = 0$, 0.5, and 1.0) converting the system from FAD to FAD$^-$. Three windows were expected to be sufficient for the free energy calculation due to the expected linear response of the solvent.[36,35] The free energy derivative was then integrated to determine the free energy change.

Using a modified QM/MM potential, thermodynamic integration calculations for the reduction of FAD were carried out using the dual topology single coordinate (DTSC) approach; the DTSC method has been recently described in detail[35] and will only be briefly summarized here. This approach combines the ideas of the dual-topology and single topology schemes into an approach that describes the system with two electronic Hamiltonians and one set of coordinates at each time step. A series of simulations convert the potential energy of the system from $\lambda = 0$ (A = FAD) to $\lambda = 1$ (B = FAD$^-$) where the QM/MM potential of the system is defined as

$$U(\mathbf{X}_A,\mathbf{X}_B,\mathbf{X}_C) = (1-\lambda)\langle\Phi_A|\hat{H}_{AA}(\mathbf{X}_A) + \hat{H}_{AC}(\mathbf{X}_A,\mathbf{X}_C)|\Phi_A\rangle + \lambda\langle\Phi_B|\hat{H}_{BB}(\mathbf{X}_B) + \hat{H}_{BC}(\mathbf{X}_B,\mathbf{X}_C)|\Phi_B\rangle + U_{CC}(\mathbf{X}_C) \quad (7)$$

where A, B, and C correspond to FAD, FAD$^-$, and TIP3P water, respectively. The QM/MM interaction energies do not depend on λ and the free energy derivative is determined from eq 7. If the same set of vdW parameters are used for the interaction between the MM and the two QM states, only the electrostatic term contributes explicitly to the free energy derivative

$$\frac{\partial G(\mathbf{X};\lambda)}{\partial\lambda} = \left\langle\frac{\partial U(\lambda)}{\partial\lambda}\right\rangle_\lambda \quad (8)$$

$$= \langle U_{elec}^{FAD^-/MM}(\mathbf{X}_{QM},\mathbf{X}_{MM}) - U_{elec}^{FAD/MM}(\mathbf{X}_{QM},\mathbf{X}_{MM})\rangle_\lambda \quad (9)$$

where $U_{elec}^{FAD/MM}$ ($U_{elec}^{FAD^-/MM}$) is the total electronic energy of the model FAD (FAD$^-$) including the electrostatic interaction with the MM solvent. The value of λ defines the solute−solvent interaction for which the difference between the potential energies for both end states is averaged. The free energy of reduction is then calculated from the free energy derivative by determining the functional dependence on λ and integrating from $\lambda = 0.0$ to 1.0. As emphasized in previous work,[35−37] although a single set of coordinates is used for both electronic states at each time-step, the method is formally exact due to the state character of free energy. The error in practical simulations arises from the fact that bonds involving hydrogen were usually constrained to be the same length in both end states, which is usually of a negligible magnitude.

In addition to determining the reduction potential, entropic and enthalpic contributions to the reduction potential were calculated (see section 3 for more discussion of motivations) based on a finite difference approach assuming a linear dependence of the free energy change on temperature (285, 300, and 325 K). The entropic term was determined from the negative slope of the linear fit, as represented by the thermodynamic relationship

$$\Delta S = -\left(\frac{\partial\Delta G}{\partial T}\right)_{N,P} \quad (10)$$

and the enthalpic term was determined from the intercept of the linear fit of the temperature dependence of the free energy change. Although it is computationaly expensive, the finite difference approach provides relatively accurate estimates of thermodynamic quantities although it is clearly limited by the accuracy of the method used to determine the free energy; methods for determining the enthalpy and entropy changes have been surveyed in a recent article.[38] Once again, although the accuracy of the SCC-DFTB/MM approach is an important issue when comparing with experiment,[35,37] this study aims to determine the relative variation of observables between vdW parameter sets, and changes in entropic and enthalpic contributions allow for a more quantitative look at the free energy change.

2.4.2. Potential of Mean Force Calculations. To illustrate the effect of the vdW parameters on QM/MM calculations of chemical reactions, the potential of mean force (PMF) for the proton transfer in a model enediolate molecule in water was studied. As discussed in previous work, this model was motivated by a possible step in the catalytic cycle of triose-

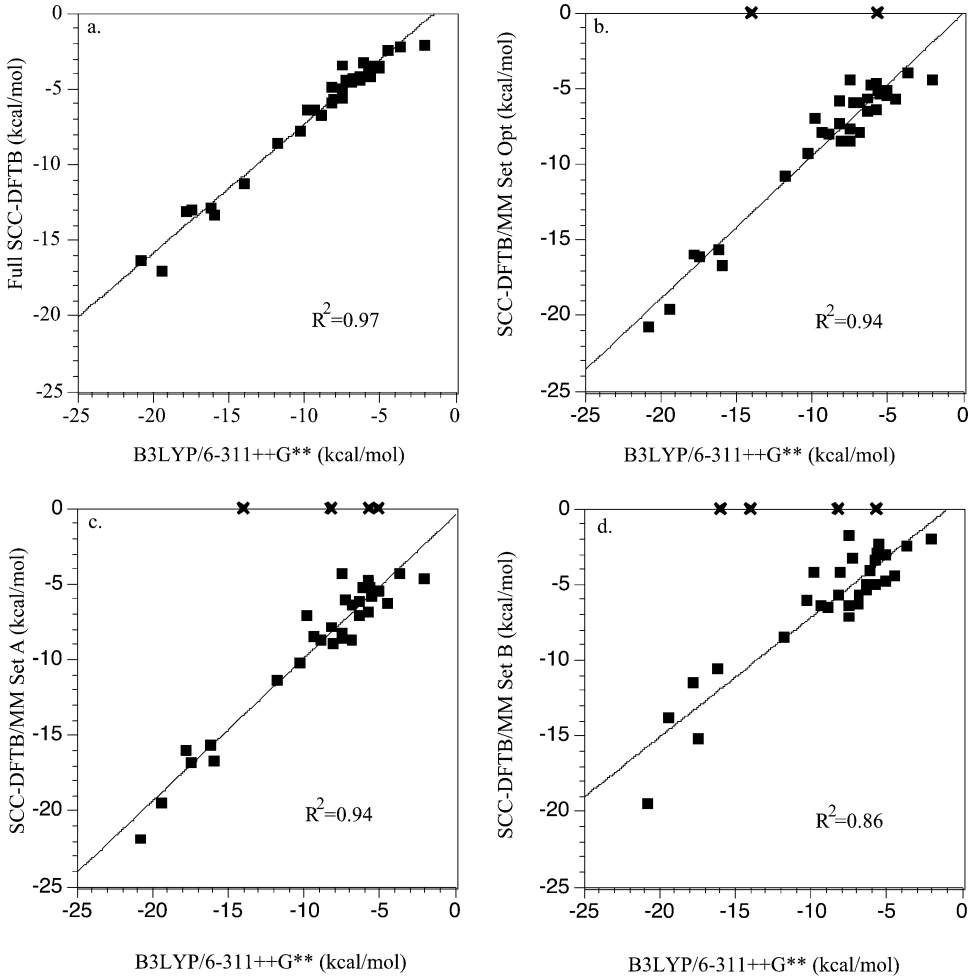

Figure 3. Interaction energies for the full SCC-DFTB and SCC-DFTB/MM with different van der Waals parameters (set Opt, A, and B) plotted against the B3LYP results. The direct comparison between B3LYP/6-311++G** interaction energies plotted on the *x*-axis and the (a) full SCC-DFTB, (b) SCC-DFTB/MM set Opt, (c) SCC-DFTB/MM set A, and (d) SCC-DFTB/MM set B. Those values for the SCC-DFTB/MM interaction energy equal to zero correspond to the stationary points not observed (see text).

phosphate isomerase.[39] As a first approximation, adiabatic maps and PMF profiles were compared for the three sets of vdW parameters in the presence of water in a 30 Å box with periodic boundary conditions applied. The adiabatic map consisted of energy minimizations along the reaction pathway, as defined by the difference between O_1-H and $H-O_2$ distances as the proton shifts from one oxygen to the other (Scheme 2). Then for each set of vdW parameters, PMF calculations were carried out with a set of SCC-DFTB/MM CPT molecular dynamics simulations with umbrella sampling[40] along the same proton-transfer reaction coordinate ($\delta = r_{O_1-H} - r_{H-O_2}$)

$$W(\delta) = -k_B T \ln \rho(\delta) \qquad (11)$$

where $W(\delta)$ depends on temperature and the probability distribution ($\rho(\delta)$) of observing the system along the reaction coordinate. To prepare the system, an unconstrained enediolate system was heated and equilibrated for 50 ps, and then a series of 50 ps simulations with harmonic potentials applied to restrain the transfer proton at different points along the reaction coordinate were carried out. The actual distances between enediolate oxygens and the transfer proton were recorded at each step for all windows, and the weighted histogram analysis method (WHAM)[41] was used to determine the PMF along the approximate reaction coordinate, δ.

3. Results and Discussion

3.1. Gas-Phase Comparisons. *3.1.1. Hydrogen Bonding Complexes.* Overall, the optimized parameters for SCC-DFTB atoms were found to increase the accuracy of predicted gas-phase hydrogen bond lengths and interaction energies when compared to the two extreme parameter sets (A and B) taken from the CHARMM22 force field; the optimized parameters were found to be transferrable when applied to the set of molecules not included in the training set (Figure 2).

More specifically, the optimized parameters recognized more of the reference stationary points than either of the other two parameter sets (Figure 3). For the training set of complexes, the RMS error in the hydrogen bond distance (interaction energy) was 0.08 (1.2), 0.10 (1.2), and 0.40 (3.4)Å (kcal/mol) for set Opt, set A, and set B respectively (Table 3). Similar results were found when the parameters were applied to the set of molecules not included in the optimization set (Table 3). All RMS calculations only included complexes with SCC-DFTB/MM stationary points. Parameter set Opt failed to locate stationary points corresponding to molecules 6 and 23 (Figure 1 and Figure 2); parameter set A failed to locate stationary points for molecules 6, 21, 23, and 33; parameter set B failed to locate stationary points for molecules 6, 11, 23, and 33. For the three sets, molecule 6 shifted the in-plane water to a configuration similar to molecule 5, but with the water at a further distance and rotated into the same plane as the carbocation containing

TABLE 1: van der Waals (vdW) Parameter Sets for SCC-DFTB Atoms in SCC-DFTB/MM Calculations

atom	set Opt[a] (Å)	set Opt[a] (kcal/mol)	set A[b] (Å)	set A[b] (kcal/mol)	set B[b] (Å)	set B[b] (kcal/mol)
C	1.70	−0.160	1.71	−0.110	2.68	−0.002
O	1.85	−0.067	1.70	−0.160	2.37	−0.001
N	1.92	−0.110	1.85	−0.200	2.15	−0.100
H	0.28	−0.039	0.23	−0.100	1.49	−0.008

[a] Optimized set of vdW parameters from the current work. [b] Extreme parameter sets selected from the CHARMM22 forcefield. Set A (set B) was selected to minimize (maximize) the hard sphere radius and maximize (minimize) the well depth.

TABLE 2: Hydrogen Bond Interaction Energies (Distances) for the Set of Complexes Used for Optimization (1−18) and Testing (19−33) at Different Levels of Calculation[a]

	B3LYP[b]	SCC-DFTB	set Opt[c]	set A[c]	set B[c]
1	−4.5 (1.99)	−2.4 (2.03)	−5.7 (1.90)	−6.2 (1.84)	−4.4 (1.88)
2	−7.5 (1.91)	−3.4 (2.01)	−4.4 (1.88)	−4.3 (1.86)	−1.7 (2.46)
3	−7.5 (1.85)	−5.0 (1.87)	−7.6 (1.81)	−8.2 (1.75)	−6.3 (1.82)
4	−5.1 (2.06)	−3.4 (1.98)	−5.4 (1.89)	−5.4 (1.90)	−3.0 (2.59)
5	−17.8 (3.37)	−13.1 (3.28)	−15.9 (3.37)	−16.0 (3.38)	−11.4 (3.92)
6	−14.0 (1.85)	−11.2 (1.80)			
7	−5.8 (1.93)	−4.2 (1.90)	−6.3 (1.87)	−6.8 (1.81)	−5.0 (1.84)
8	−10.3 (1.79)	−7.7 (1.81)	−9.2 (1.79)	−10.2 (1.77)	−6.0 (1.86)
9	−3.7 (2.05)	−2.2 (2.02)	−3.9 (2.02)	−4.3 (1.93)	−2.4 (1.96)
10	−19.5 (1.70)	−17.0 (1.67)	−19.5 (1.68)	−19.4 (1.70)	
11	−16.0 (2.76)	−13.3 (2.63)	−16.6 (2.78)	−16.6 (2.80)	−13.8 (3.08)
12	−7.3 (1.93)	−4.4 (2.01)	−5.9 (2.02)	−6.0 (2.03)	−3.2 (2.26)
13	−5.8 (1.99)	−3.9 (1.93)	−4.6 (1.85)	−4.7 (1.86)	−3.3 (2.54)
14	−17.5 (1.67)	−13.0 (1.72)	−16.1 (1.79)	−16.8 (1.73)	−15.1 (1.77)
15	−20.8 (3.17)	−16.3 (3.04)	−20.7 (3.07)	−21.8 (3.02)	−19.4 (3.10)
16	−16.2 (1.73)	−12.8 (1.75)	−15.6 (1.72)	−15.6 (1.73)	−10.5 (2.60)
17	−5.6 (1.92)	−3.5 (1.88)	−5.3 (1.79)	−5.8 (1.76)	−2.3 (2.53)
18	−6.1 (1.88)	−3.2 (1.91)	−4.7 (1.87)	−5.2 (1.81)	−4.0 (1.90)
19	−6.4 (1.92)	−4.4 (1.89)	−6.5 (1.90)	−7.0 (1.84)	−5.0 (1.85)
20	−8.1 (1.84)	−5.6 (1.85)	−8.4 (1.75)	−8.9 (1.72)	−4.1 (2.48)
21	−5.1 (1.99)	−3.6 (1.93)	−5.1 (1.87)		−4.8 (1.89)
22	−11.8 (1.83)	−8.5 (1.93)	−10.8 (1.85)	−11.4 (1.78)	−8.4 (1.81)
23	−5.7 (1.92)	−4.1 (1.89)			
24	−9.9 (1.97)	−6.3 (1.96)	−6.9 (2.15)	−7.1 (2.15)	−4.2 (2.33)
25	−6.9 (1.86)	−4.3 (1.88)	−5.9 (1.82)	−6.4 (1.76)	−5.6 (1.84)
26	−6.9 (1.87)	−4.5 (1.92)	−7.9 (1.78)	−8.7 (1.72)	−6.2 (1.81)
27	−6.4 (1.89)	−4.1 (1.89)	−5.6 (1.84)	−6.1 (1.77)	−5.3 (1.85)
28	−9.4 (1.90)	−6.3 (1.89)	−7.9 (1.87)	−8.4 (1.80)	−6.4 (1.84)
29	−5.7 (2.00)	−3.5 (1.95)	−5.1 (1.88)	−5.2 (1.89)	−2.9 (2.57)
30	−7.5 (2.13)	−5.6 (2.07)	−8.4 (2.01)	−8.6 (2.02)	−7.1 (1.87)
31	−8.9 (1.89)	−6.7 (1.88)	−8.0 (1.85)	−18.7 (1.77)	−6.5 (1.80)
32	−8.2 (1.92)	−5.9 (1.91)	−7.3 (1.88)	−7.8 (1.81)	−5.7 (1.83)
33	−8.2 (2.08)	−4.9 (2.03)	−5.8 (2.13)		

[a] The interaction energies were calculated adiabatically and are given in kcal/mol; the distances are given in Å. [b] Basis set for energy evaluation//geometry optimization is 6-311++G(d,p)//6-31+G(d,p). [c] Stationary points not observed are denoted by empty entries.

the lysine analogue (Figure 1). For all three sets the starting geometry of molecule 23 minimized to molecule 24 (Figure 2). For set A, molecule 21 minimized to 19; for set B molecule 11 minimized to molecule 10.

The SCC-DFTB/MM with optimized vdW parameters was found to yield more accurate hydrogen bond interaction energies but less accurate geometries than the full SCC-DFTB when compared to the reference results from B3LYP calculations. The full SCC-DFTB hydrogen bond interaction energies were underestimated by about 2−3 kcal/mol yielding an RMS of 3.0 kcal/mol for the training set, while the geometries were the most accurate compared to the reference geometries yielding an RMS of 0.07 Å for the hydrogen bond lengths (Table 3).

Although interaction energies and bond lengths improved for the optimized set of vdW parameters, the angles did not (which most likely contributes to the inability to recognize some stationary points) and still remain a limitation for the SCC-DFTB/MM approach due to the coupling between the quantum and molecular mechanics regions. As mentioned above (eq 4), SCC-DFTB/MM uses the Mulliken partial charges to determine the electrostatic interaction between the QM and MM atoms[14] and, thus, ignores the shape of the QM molecular orbitals. As a result, the anisotropy of the QM/MM interactions is underestimated with the current implementation. An improved SCC-DFTB/MM approach with an orbital description, e.g., using the analytical one-electron operator for the interaction between the QM electrons and MM partial charges as in most ab initio or DFT based QM/MM implementations[5,42] may improve bond angles for the gas phase, but this may prove to be of limited practical value when applied to condensed phase systems. Future work will investigate this issue further.

TABLE 3: RMS Errors for Interaction Energy and Hydrogen Bond Length of SCC-DFTB and SCC-DFTB/MM Compared to B3LYP[a] Reference Values Determined for the Set of Complexes Used for Optimizing (Testing) the van der Waals Parameters

calculation	interaction energy (kcal/mol)	hydrogen bond length (Å)
SCC-DFTB	3.0 (2.5)	0.07 (0.04)
SCC-DFTB/MM set Opt	1.2 (1.2)	0.08 (0.09)
SCC-DFTB/MM set A	1.2 (1.1)	0.10 (0.12)
SCC-DFTB/MM set B	3.4 (2.5)	0.40 (0.27)

[a] Basis set for energy evaluation//geometry optimization is 6-311++G(d,p)//6-31+G(d,p). The RMS calculations for SCC-DFTB/MM do not include values for the stationary points that were not observed; Set Opt:6 and 23; set A: 6, 21, 23, and 33; set B: 6, 11, 23, and 33.

3.1.2. FAD Water Cluster. The results of the potential energy difference calculations for a small water FAD cluster with full SCC-DFTB and SCC-DFTB/MM (set Opt, set A, and set B) were carried out to compare the interaction of water molecules with isoalloxazine treated at the full SCC-DFTB level to the SCC-DFTB/MM treatment where the isoalloxazine is treated with SCC-DFTB and the waters are described by a modified TIP3P model. The initial cluster was taken from a SCC-DFTB/MM (set Opt) molecular dynamics snapshot, including all waters within 3.0 Å of the neutral isoalloxazine. See the Supporting Information for the relaxed cluster geometries. The clusters were then minimized with the three vdW parameter set SCC-DFTB/MM and full SCC-DFTB for the neutral and reduced isoalloxazine in order to qualitatively compare observable interactions that would be present during a typical MD simulation. Overall the optimized parameters performed best in predicting the full SCC-DFTB hydrogen bond lengths and reduction potential with the smallest deviation for the reduction potential of −4.7 kcal/mol as compared the −5.3 and +7.0 kcal/mol for set A and set B, respectively (Table 4). The very large change in the reduction potential for set B was due to the different hydrogen bonding environment around the model FAD upon geometry minimization.

3.2. Condensed Phase Observables. The most relevant application and test for the SCC-DFTB/MM is in the condensed phase, and this investigation is intended to determine the magnitudes of difference that the vdW parameters for SCC-DFTB atoms can be reflected in condensed phase observables. Overall, there were differences observed between parameter sets for the condensed phase observables, and the expected trend of

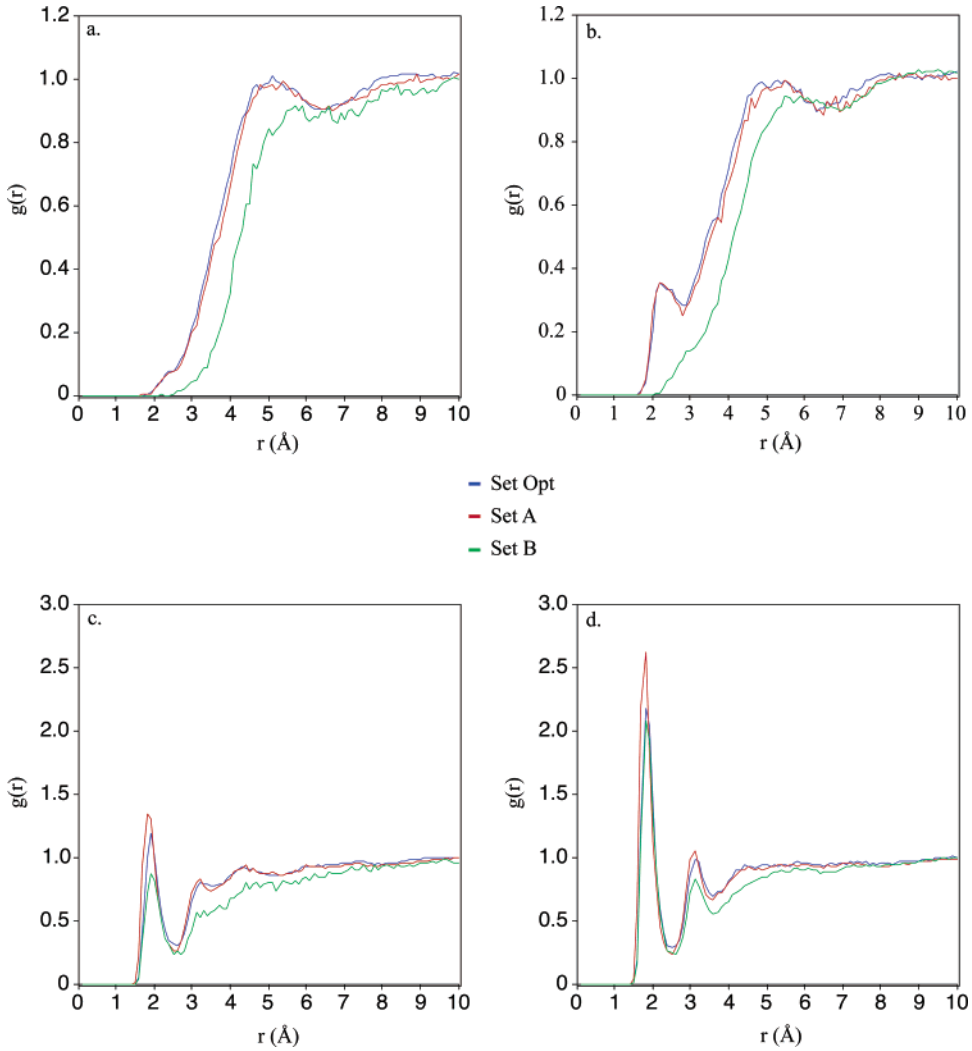

Figure 4. Radial distribution functions of TIP3P waters about the model FAD molecule (7,8-dimethyl isoalloxazine). The distributions of TIP3P hydrogens about (a,b) C7 and (c,d) Ob (Scheme 1) for the (a,c) neutral and (b,d) reduced states of FAD calculated from SCC-DFTB/MM CPT molecular dynamics with periodic boundary conditions. Each production run consisted of about 600 ps (see section 2 for details).

TABLE 4: Comparison of the Gas Phase Potential Energy Changes with the QM/MM Free Energy for the Reduction of FAD[a] in the Condensed Phase Calculated with Three Sets of vdW Parameters

calculation	ΔE gas phase, kcal/mol	ΔE cluster,[c] kcal/mol	ΔG at 300 K, kcal/mol	ΔS[d], cal/mol	ΔH[d], kcal/mol
B3LYP[b]	-44.8				
SCC-DFTB	−37.3	−58.7			
set Opt		−54.0	−70.9	−12.4	−74.6
set A		−53.4	−72.1	−10.2	−75.0
set B		−65.7	−68.7	−15.1	−73.3

[a] 7,8-Dimethyl isoalloxazine was used as an FAD analog. [b] Basis set for energy evaluation//geometry optimization is 6-311++G(d,p)//6-31+G(d,p). [c] The initial geometry for the small cluster calculations was taken from a set Opt SCC-DFTB/MM molecular dynamics snapshot including the nearest 15 water molecules. The initial structure was then relaxed for the neutral and reduced states of FAD for each parameter set and the energy difference between both states was determined. [d] The changes in the entropic and enthalpic terms were determined from the linear fit for the free energy change as a function of temperature; the entropy change was determined from the negative of the slope, and the enthalpy change was determined from the intercept.

observables for the optimized parameter set being sandwiched between the two extreme sets was seen; the radial distribution functions indicated the tightest solvation for set A and the losest solvation with a loss of specificity for set B. The free energy and PMF results were, by contrast, less sensitive to the vdW parameters; the free energy and PMF were even reasonable for set B, which fell within 2 kcal/mol of the optimized values.

3.2.1. Radial Distribution Functions. Investigations of radial distribution functions, $g(r)$, about different solute atoms can provide insights into changes in local solvent structure due to differences in the overall QM/MM interaction potential. In this study, we calculated radial distribution functions of TIP3P water molecules about the neutral and reduced states of the model FAD as well as an enediolate to determine the effects of different vdW parameters for the QM atoms and chemical states of the solute on the distribution of waters. For FAD, the radial distributions about a hydrophobic carbon atom (C7, Scheme 1) and hydrophillic carbonyl oxygen (Ob, Scheme 1) are discussed here; other radial distribution plots have been included in the Supporting Information. For the enediolate radial distributions about the hydroxyl oxygen and transferring proton along with the proton accepting carbonyl oxygen are discussed here.

Noticeable differences between vdW parameter sets for radial distributions of water molecules about the neutral and reduced states of the FAD are observed. The distribition of water molecules about C7 in FAD (Scheme 1) are similar for both the set Opt and set A, whereas the first peak (2.1 Å) is lost for the set B simulation (Figure 4b); set B pushes the distributions out by about 1.0 Å for both the neutral and reduced states of

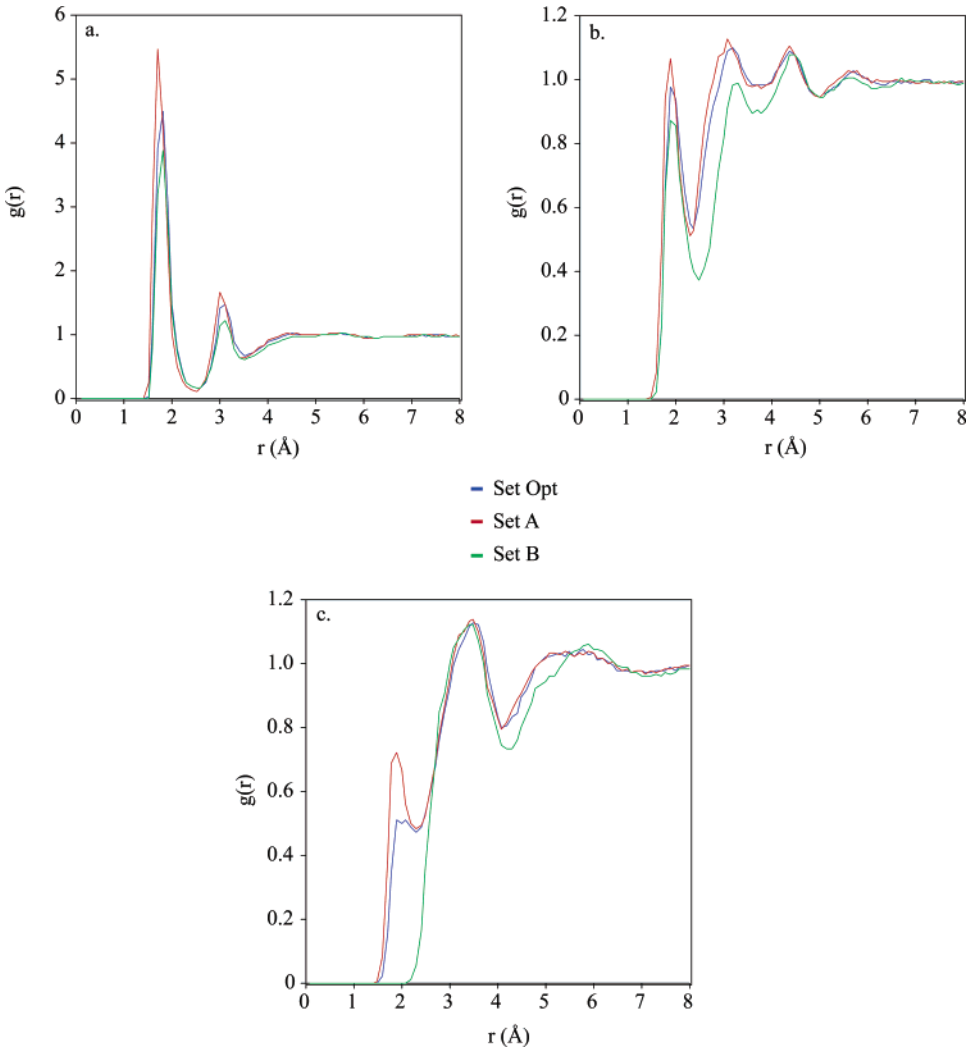

Figure 5. Radial distribution functions of TIP3P water about an enediolate (Scheme 2). The distribution of (a) TIP3P hydrogens about the carbonyl O, (b) TIP3P oxygens about the transfer protons, and (c) TIP3P hydrogens about the hydroxyl oxygen were calculated from SCC-DFTB/MM CPT molecular dynamics with periodic boundary conditions for the three van der Waals parameter sets. Each production run consisted of about 2 ns (see section 2 for details).

FAD (Figure 4a,b). For the distribution of water molecules about the reduced FAD oxygen atom (Ob in Scheme 1), set A has the highest number of water molecules in the first peak (2.6), whereas the set Opt has a peak height of 2.2 and set B 2.1 (Figure 4d); there is a slight shift of the set A peak to a shorter distance when compared to set Opt and set B, revealing a tighter first solvation shell. A similar shift was determined for distribution of water molecules about the caboxyl oxygen of neutral FAD for set A (Figure 4c). The differences between the peak heights for set Opt and set B are more substantial about the Ob of the neutral FAD. Similar differences are seen for the second peak between set A and set Opt, while for set B, the peaks are significantly reduced.

Similar trends were found for the distribution of water molecules about enediolate (Scheme 2). For the distribution of water molecules about the carbonyl oxygen (Figure 5a), the first solvation shell for set Opt and set B are again shifted outward (by about 0.2 Å) relative to set A, and the peak heights are again lower than set A (with set A at 5.5, set Opt at 4.5, and set B at 3.9). Similar shifts and differences in peak height are observed in the second peak. Similar trends can be seen in the distribution of water about the transferring proton (Figure 5b); the overall distribution for set B has been shifted much lower for the first two peaks. For the distribution of water about the hydroxyl oxygen, the first peak observed for set A and set Opt was not present at all for set B (Figure 5c).

3.2.2. FAD Reduction Potential. For the reduction of FAD, it is interesting to consider the differences in charge distributions between the neutral and reduced states. If the addition of one electron was fairly localized, say about one atom, then the Born model[43,44] of solvation may be used to crudely estimate the free energy associated with charging the FAD from the neutral to reduced state in solution. When considering the role of FAD in protein systems, it seems unlikely that such localized charges would be observed. FAD spreads the electron density over its highly conjugated ring structure, and indeed, the Mulliken partial charge analysis of FAD in small water clusters yields a fairly spread out electron distribution; therefore, other approaches to calculating the solvation free energy change must be considered.[36] In this study, we determine the free energy required to charge up a FAD molecule in solution and its dependence on the vdW parameters for SCC-DFTB atoms. As mentioned above, the DTSC approach proves to be very convenient here since the initial and final states of the molecule are very similar; an example of the convergence of the free energy derivative along with the linear fit of its converged values are shown in Figure 6. Overall, the reduction potential was found to be fairly insensitive to the vdW parameter sets (ranging from −68.7 for

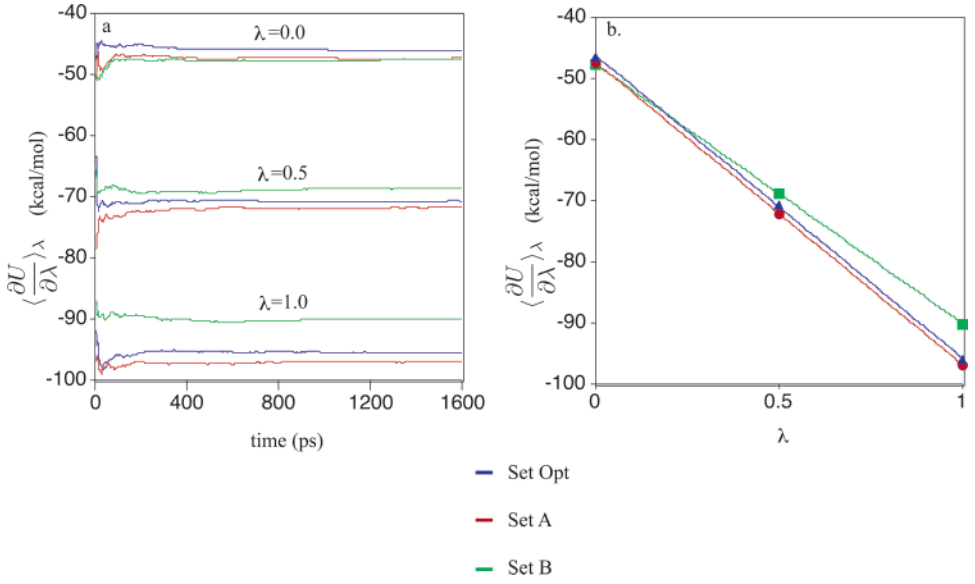

Figure 6. Examples of the free energy derivative convergence and integration. (a) The convergence of the free energy derivative is plotted as a function of time; these calculations were run at 300 K with SCC-DFTB/MM CPT molecular dynamics with peridic boundary conditions applied. (b) A plot of the converged free energy derivative for the three perturbative steps. Integration of the equation for the linear fit from $\lambda = 0$ to 1 determines the free energy change.

SCHEME 3

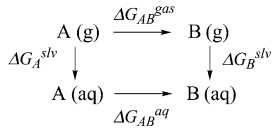

$$\Delta G_{AB}^{aq} = \Delta G_{AB}^{gas} + \Delta G_B^{slv} - \Delta G_A^{slv}$$

set B to −72.1 kcal/mol for set A) and the large deviation of the set B reduction potential observed in the gas phase FAD−water clusters reduced significantly to about 2 kcal/mol below the set Opt results (Table 4).

To further analyze the effect of van der Waals interactions on the computed reduction potential, we consider the well established thermodynamic cycle as shown in Scheme 3. Due to the state-function character of free energies, the reduction free energy in solution (ΔG_{AB}^{aq}, here A = FAD, B = FAD$^-$) is equal to the gas-phase value (ΔG_{AB}^{gas}) plus the difference in the solvation free energies ($\Delta G_{A/B}^{slv}$). Since ΔG_{AB}^{gas} does not include any MM component, the QM/MM interactions (electrostatic plus van der Waals) influence ΔG_{AB}^{aq} via the solvation free energies. Because FAD$^-$ is better solvated than the charge neutral FAD, it is not surprising that the reduction free energy is about 30 kcal/mol more favorable in the condensed phase than in the gas phase (Table 4). Furthermore, as discussed above, set A in general has the tightest solvent structure around the solute, whereas set B has the loosest solvation structure; thus, it is expected that set B has the smallest solvation contribution and therefore the smallest increase in reduction free energy upon solvation; this is indeed what was found here, as set B has a lower reduction free energy than set A and set Opt by 3.4 and 2.2 kcal/mol, respectively (Table 4).

It is interesting to further explore the origin of the weak dependence of the reduction potential on the QM vdW parameters. It could be a simple consequence of error cancellation; that is, errors in the solvation free energies of A and B cancel out in computing ΔG_{AB}^{aq}. Alternatively, it is possible that enthalpy−entropy compensation[45,46] makes solvation free energies of both A and B rather insensitive to the QM vdW parameters. Instead of explicitly computing solvation free energies, we restrict ourselves here to an estimate of enthalpic and entropic components of the reduction free energy in solution with different QM vdW parameters. If enthalpy−entropy compensation plays a major role, we expect that the variation in the enthalpic/entropic component with QM vdW parameters is larger compared to that in the reduction free energy.

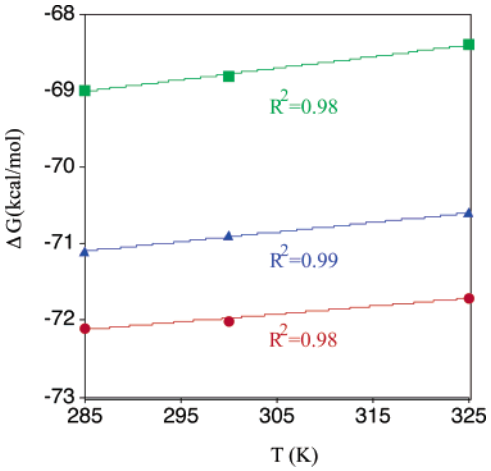

Figure 7. Plot of the temperature dependence of the free energy used to determine entropic and enthalpic contributions to the reduction of FAD.

As shown in Figure 7 and Table 4, for all three parameter sets, the entropy was found to decrease while the enthalpic term became more negative upon reduction as is consistent with this exothermic process. Parameter set B has the smallest enthalpic change and the largest entropic change leading to the smallest free energy change overall (Table 4). The qualitative differences between parameter sets for the enthalpy and entropy are consistent with expectation. The favorable enthalpic term is due to the stronger interaction of the solvent molecules with the reduced FAD, whereas the negative entropy change implies that the solvent in the charged (FAD$^-$) system is more restricted configurationally. Set B has the largest entropy change because the negative charge of FAD$^-$ has the largest effect relative to the neutral state in pulling solvent molecules closer as compared to set A and set Opt; thus, the overall change in configurational flexibility is greatest for set B. Quantitatively, the variations in

TABLE 5: Comparison of the B3LYP Gas Phase Potential Energy Barrier with the Condensed Phase QM/MM Free Energy Barriers, Calculated with Three Sets of van der Waals Parameters, for the Intramolecular Proton Transfer in Enediolate

	gas phase (kcal/mol)	adiabatic map[c] (kcal/mol)	PMF[c] (kcal/mol)
B3LYP[a]	8.7 [9.5]		
SCC-DFTB	8.2		
set Opt[b]		9.8	9.2
set A[b]		10.4	9.8
set B[b]		10.4	8.5

[a] Basis set for energy evaluation//structure optimization was 6-311+G(d,p)//6-31+G(d,p). [b] SCC-DFTB/TIP3P calculations using different set of van der Waals parameters for the SCC-DFTB atoms. [c] The approximate reaction coordinate is the anti-symmetric stretch involving the donor oxygen, transferring proton and the acceptor oxygen (see text and Fig. 8). The adiabatic map was generated using a random solvent configuration collected from a CPT MD simulation, and the PMF was generated using umbrella sampling with CPT MD simulations (see text for more details).

the enthalpy and entropy are smaller than that in the free energy, e.g., the reduction free energy of the optimized set is approximately 1 kcal/mol less favorable than set A, consisting of a 0.6 kcal/mol of entropic and 0.4 kcal/mol of enthalpic contribution. Therefore, it seems unlikely that enthalpy−entropy compensation is a major effect here, and error cancellation is the main origin behind the weak dependence of the reduction free energy on QM vdW parameters. Explicit exploration of the dependence of QM/MM solvation free energy on QM vdW parameters will be carried out to verify this point in the future.

Finally, an additional reduction potential simulation was run at 300 K using set B with a switch to the optimized parameters for only the carbon atoms. The resulting reduction potential was ~ -70.7 kcal/mol, only 0.2 kcal/mol less favorable than the optimized result. This is reasonable when considering the extra charge is spread throughout the molecule and as most of the molecule consists of carbon atoms, a change in the carbon parameters would have the largest effect.

3.2.3. Potential of Mean Force. Similar to the reduction potentials, the PMF curves were found to be fairly insensitive to the vdW parameter set, yielding very similar barriers and shapes. There are some noticeable differences that were consistent with the trends observed in the radial distribution and free energy calculations: the optimized set falls between the set B and set A result as expected. The free energy barriers (8.5, 9.2, and 9.5 kcal/mol for sets B, Opt, and A, Table 5) are all slightly higher than the gas-phase potential barrier (8.2 kcal/mol). Set B yielded the lowest barrier (8.5 kcal/mol), and shortest reaction path with minima at around ±1.2 Å (Figure 8). Set A yielded the highest barrier (9.8 kcal/mol) with the broadest reaction path where the minima are at around ±1.5 Å (Figure 8). Set Opt yielded a barrier 0.7 kcal/mol above set B and 0.6 kcal/mol below set A with minima at around ±1.4 Å (Figure 8). These results imply that the tighter the solvation of the enediolate the more difficult it is to transfer the proton within the molecule. This is supported by the radial distribution functions of water molecules about the acceptor oxygen (Figure 5a). The acceptor oxygen has from 3.5 to 5.5 TIP3P hydrogens in the first peak, at 1.9 Å, whereas the hydroxyl oxygen has far fewer and is even lacking in set B (Figure 5c).

4. Concluding Remarks

Hybrid QM/MM approaches are, in principle, powerful techniques for exploring chemical events in complex molecular

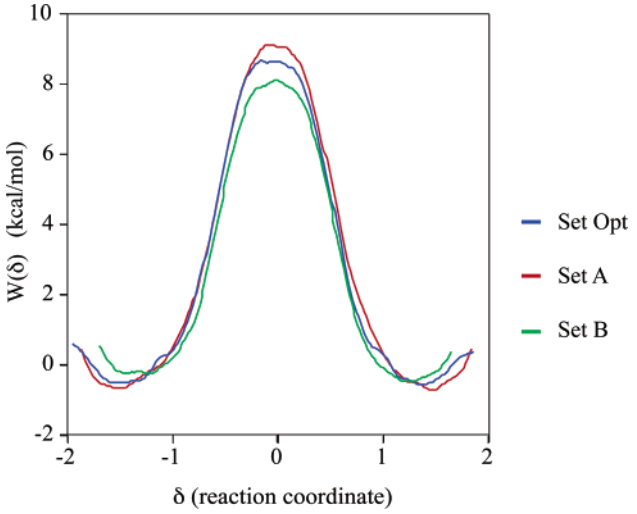

Figure 8. Potential of mean force for the intramolecular proton transfer in an enediolate. A series of umbrella sampling simulations were run to determine the effect of the van der Waals parameter set for SCC-DFTB atoms on the PMF where the reaction coordinate is taken to be δ, which is the anti-symmetric stretch involving the two oxygen atoms and the proton (see text).

environments. The practical value of QM/MM simulations, however, may depend critically on many parameters such as the treatment of long-range electrostatics and the amount of conformational sampling. The details of interaction between the QM and MM atoms, which often includes both electrostatic and van der Waals components, certainly may have a large impact on the accuracy of the final results. In this investigation, we explored the importance of van der Waals interactions on the results of QM/MM simulations with an approximate density functional theory (SCC-DFTB) coupled to the TIP3P water model as an example. First, the vdW parameters for SCC-DFTB atoms were optimized for use in SCC-DFTB/MM calculations. The vdW parameters were found to be transferable to hydrogen bonding interactions in molecules not included in the training set of molecules. The effects of different vdW parameters for SCC-DFTB atoms were tested in the gas and condensed phase by using three different parameter sets. It was found that, although there were noticeable differences between solvent radial distribution functions around the solute for the three vdW parameters sets, overall the variations in thermodynamic quantities (reduction free energy of a model FAD and potential of mean force for a proton transfer) were rather small. Nevertheless, the observed trends in the simulation results are not random. The condensed phase observables for set Opt are always flanked by set B and set A: radial distribution functions are pushed out for set B and pulled into the solute for set A. Set B yielded the lowest, whereas set A yielded the highest reduction potential for FAD due to differences in stabilization of the reduced state by the solvent, and set B yielded the lowest barrier, whereas set A yielded the highest for the intramolecular proton transfer in enediolate as can be understood in terms of the tighter solvation shell about the acceptor oxygen. The free energy of reduction was decomposed into enthalpic and entropic contributions, and set B yielded a less favorable enthalpy and entropy change for the reduction of FAD due the balancing of the repulsive vdW parameters and the electrostatic interactions of the solvent with either the neutral or reduced state of FAD. These observations indicate that it is unlikely that enthalpy−entropy compensation plays a major role and it is simply cancellation of errors in solvation energies (see Scheme 3) that

makes relative thermodynamic quantities depend weakly on the QM vdW parameters.

Although the results reported here were obtained using the SCC-DFTB/MM potential, the qualitative conclusions are likely to be applicable to QM/MM simulations in general. The results provide some leniency in the choice of vdW parameters when applying QM/MM to condensed phase systems, although one should always be careful in the selection of parameters to retain physical reality, especially when considering some of the changes to the radial distribution functions calculated with the set B parameters. Moreover, considering the rapid variation of the van der Waals interactions, it is also likely that the choice of QM/MM vdW parameters has a significant effect on dynamical observables, such as the rate of vibrational relaxation in the condensed phase;[47] this will be investigated systematically in the future.

Finally, it is useful to briefly summarize the applicability of the SCC-DFTB and SCC-DFTB/MM approach in the current form, which appear to be more reliable than methods based on traditional semiempirical methods in many systems tested so far.[14,48−50,18,51,52] As to the full SCC-DFTB, both previous[53] and current benchmark calculations indicate that it is very reliable for hydrogen bonding geometries (including angles), although it tends to systematically underestimate the energetics of hydrogen bonding interactions by 2−3 kcal/mol. With a reasonable set of van der Waals parameters, SCC-DFTB/MM produces both reliable geometries and energetics for hydrogen bonding type of interactions, with errors in energetics even smaller than that of full SCC-DFTB for the systems tested here. Therefore, we expect that SCC-DFTB/MM is well suited for studying energetics associated with chemical processes occurring in polar environments (such as water and biomolecules), as far as the van der Waals parameters for the SCC-DFTB atoms do not take extreme values. The current study made it clear that to improve the reliability of SCC-DFTB/MM method efforts should be focused on components other than the van der Waals interaction. First, it is worth going beyond the Mulliken charge representation for the QM/MM electrostatic interaction, which might improve the anisotropy of such interactions. Second, especially in applications where nonpolar effects might be important, dispersion interactions among SCC-DFTB atoms should be taken into account.[15] Finally, to study chemical processes in complex environments such as protein−nucleic-acid complexes or systems embedded in lipid membranes, it is crucial to construct efficient algorithms for describing interactions between SCC-DFTB atoms and the environment. These areas are being actively pursued in our research group.

Acknowledgment. We thank Mr. A. Van Wynsberghe for participating some in of the benchmark calculations in the beginning stage of the project and for a careful reading of the manuscript. The Q.C. group is partially supported by the starting-up fund from the Department of Chemistry and College of Letters and Science at University of Wisconsin, Madison, a PRF-G grant administered by the American Chemical Society, a Research Innovation Award from the Research Corporation, and grants from the National Science Foundation (MCB-0314327, CHE-CAREER-0348649). Q.C. is a Alfred P. Sloan Research Fellow.

Supporting Information Available: Optimized structures of the gas-phase cluster formed by the model FAD and water molecules at various SCC-DFTB and SCC-DFTB/TIP3P levels are shown. Additional radial distribution functions for water molecules around atoms in the model FAD calculated from SCC-DFTB/TIP3P simulations are also included. This material is available free of charge via the Internet at http://pubs.acs.org.

References and Notes

(1) Head-Gordon, M. *J. Phys. Chem.* **1996**, *100*, 13213−13225.
(2) Gogonea, V.; Suarez, D.; van der Vaart, A.; Merz, K. W. *Curr. Opin. Struct. Biol.* **2001**, *11*, 217−223.
(3) Warshel, A. *Computer Modeling of Chemical Reactions in Enzymes and Solution*; Wiley: New York, 1991.
(4) Field, M. J.; Bash, P. A.; Karplus, M. *J. Comput. Chem.* **1990**, *11* (6), 700−733.
(5) Lipkowitz, K. B., Boyd, D. B., Gao, J., Eds.; *Reviews in Computational Chemistry VII*; VCH: New York, 1995.
(6) Warshel, A. *Annu. Rev. Biophys. Biom.* **2003**, *32*, 425−443.
(7) Reuter, N.; Dejaegere, A.; Maigret, B.; Karplus, M. *J. Phys. Chem. A* **2000**, *104*, 1720−1735.
(8) Gao, J.; Amara, P.; Alhambra, C.; Field, M. J. *J. Phys. Chem. A* **1998**, *102*, 4714−4721.
(9) Bash, P. A.; Ho, L. L.; A. D. M., Jr.; Levine, D.; Hallstrom, P. *Proc. Natl. Acad. Sci.* **1996**, *93*, 3698−3703.
(10) Freindorg, M.; Gao, J. *J. Comput. Chem.* **1996**, *17* (3), 386-395.
(11) Luque, F. J.; Reuter, N.; Cartier, A.; Ruiz-Lopez, M. F. *J. Phys. Chem. A* **2000**, *104*, 10923−10931.
(12) Murphy, R. B.; Phillipp, D. M.; Friesner, R. A. *J. Comput. Chem.* **2000**, *21*, 1442−1457.
(13) Elstner, M.; Porezag, D.; Jungnickel, G.; Elstner, J.; Haugk, M.; Frauenheim, T.; Suhai, S.; Seifert, G. *Phys. Rev. B* **1998**, *58* (11), 7260−7268.
(14) Cui, Q.; Elstner, M.; Kaxiras, E.; Frauenheim, T.; Karplus, M. *J. Phys. Chem. B* **2001**, *105* (2), 569−585.
(15) Elstner, M.; Hobza, P.; Frauenheim, T.; Suhai, S.; Kaxiras, E. *J. Chem. Phys.* **2001**, *114* (12), 5149−5155.
(16) Li, G.; Cui, Q. *J. Am. Chem. Soc.* **2003**, *125*, 15028−15038.
(17) Zhang, X.; Harrison, D.; Cui, Q. *J. Am. Chem. Soc.* **2002**, *124*, 14871−14878.
(18) Elstner, M.; Cui, Q.; Munih, P.; Kaxiras, E.; Frauenheim, T.; Karplus, M. *J. Comput. Chem.* **2003**, *24*, 565−581.
(19) Reed, A. E.; Curtiss, L. A.; Weinhold, F. *Chem. Rev.* **1988**, *88*, 899−926.
(20) Brooks, B. R.; Bruccoleri, R. E.; Olafson, B. D.; States, D. J.; Swaminathan, S.; Karplus, M. *J. Comput. Chem.* **1983**, *4* (2), 187−217.
(21) A. D. M., Jr.; Bashford, D.; Bellot, M.; R. L. D., Jr.; Evanseck, J. D.; Field, M. J.; Fischer, S.; Gao, J.; Guo, H.; Ha, S.; Joseph-McCarthy, D.; Kuchnir, L.; Kuczera, K.; Lau, F. T. K.; Mattos, C.; Michnick, S.; Ngo, T.; Nguyen, D. T.; Prodhom, B.; W. E. R., III.; Roux, B.; Schlenkrich, M.; Smith, J.; Stote, R.; Straub, J.; Watanabe, M.; Wiorkiewicz-Kuczera, J.; Yin, D.; Karplus, M. *J. Phys. Chem. B* **1998**, *102*, 3586−3616.
(22) Goldberg, D. E. *Genetic Algorithms in Search, Optimization, and Machine Learning*; Addison-Wesley: Reading, MA, 1989.
(23) Becke, A. D. *Phys. Rev. A* **1988**, *38*, 3098−3100.
(24) Becke, A. D. *J. Chem. Phys.* **1993**, *98*, 5648−5652.
(25) Lee, C.; Yang, W.; Parr, R. G. *Phys. Rev. B* **1988**, *37*, 785−789.
(26) Haharan, P. C.; Pople, J. A. *Theor. Chim. Acta* **1973**, *28*, 213−222.
(27) Krishnan, R.; Binkley, J. S.; Seeger, R.; Pople, J. A. *J. Chem. Phys.* **1980**, *72*, 650−654.
(28) Sim, F.; St-Amant, A.; Papai, I.; Salahub, D. R. *J. Am. Chem. Soc.* **1992**, *114*, 4391−4400.
(29) Rablen, P. R.; Lockman, J. W.; Jorgensen, W. L. *J. Phys. Chem. A* **1998**, *102*, 3782−3797.
(30) Petersson, G. A.; Malick, D. K.; Wilson, W. G.; Ochterski, J. W.; Montgomery, J. A.; Frisch, M. J. *J. Chem. Phys.* **1998**, *109*, 10570−10579.
(31) Hobza, P.; Sponer, J. *Chem. Rev.* **1999**, *99*, 3247−3276.
(32) Carroll, D. L. http://cuaerospace.com/carroll/ga.html.
(33) Martyna, G. J.; Tobias, D. J.; Klein, M. L. *J. Chem. Phys.* **1994**, *101*, 4177−4189.
(34) Rychaert, J. P.; Ciccotti, G.; Berendsen, H. J. *J. Comput. Phys.* **1977**, *23*, 327−341.
(35) Li, G.; Zhang, X.; Cui, Q. *J. Phys. Chem. B* **2003**, *107*, 8643−8653.
(36) Dejaegere, A.; Karplus, M. *J. Phys. Chem.* **1996**, *100*, 11148−11164.
(37) Li, G.; Cui, Q. *J. Phys. Chem. B* **2003**, *107*, 14521−14528.
(38) Lu, N.; Kofke, D. A.; Woolf, T. B. *J. Phys. Chem. B* **2003**, *72*, 650−654.
(39) Cui, Q.; Karplus, M. *J. Am. Chem. Soc.* **2002**, *124*, 3093.
(40) Torrie, G.; Valleau, J. *J. Comput. Phys.* **1977**, *23*, 187−199.
(41) Kumar, S.; Bouzida, D.; Swendsen, R. H.; Kollman, P. A.; Rosenberg, J. M. *J. Comput. Chem.* **1992**, *13* (8), 1011−1021.
(42) Lyne, P. D.; Hodoscek, M.; Karplus, M. *J. Phys. Chem. A* **1999**, *103*, 3462−3471.

(43) Rashin, A. A.; Honig, B. *J. Phys. Chem.* **1985**, *89*, 5588−5593.
(44) Roux, B.; Yu, H.; Karplus, M. *J. Phys. Chem.* **1990**, *94*, 4683−4688.
(45) Qian, H.; Hopfield, J. J. *J. Chem. Phys.* **1996**, *105*, 9292−9298.
(46) Levy, R. M.; Gallicchio, E. *Annu. Rev. Phys. Chem.* **1998**, *49*, 331−367.
(47) Chesnoy, J.; Gale, G. M. *Adv. Chem. Phys.* **1988**, *70*, 297−355.
(48) Bohr, H. G.; Jalkanen, K. J.; Elstner, M.; Suhai, K. F. S. *Chem. Phys.* **1999**, *246*, 13−36.
(49) Elstner, M.; Jalkanen, K. J.; Knapp-Mohammady, M.; Frauenheim, T.; Suhai, S. *Chem. Phys.* **2000**, *256*, 15−27.
(50) Elstner, M.; Jalkanen, K. J.; Knapp-Mohammady, M.; Frauenheim, T.; Suhai, S. *Chem. Phys.* **2001**, *263*, 203−219.
(51) Zhou, H. Y.; Tajkhorshid, E.; Frauenheim, T.; Suhai, S.; Elstner, M. *Chem. Phys.* **2002**, *277*, 91−103.
(52) Elstner, M.; Frauenheim, T.; Suhai, S. J. *Mol. Struct. THEOCHEM* **2003**, *632*, 29−51.
(53) Elstner, M.; Frauenheim, T.; Kaxiras, E.; Seifert, G.; Suhai, S. *Phys. Stat. Sol. B* **2003**, *632*, 29−51.